RCS reduction by 1-bit coding metasurface

Ali Mourad, Ludovic Burgnies, Eric Lheurette

RCS reduction by 1-bit coding metasurface

Ali Mourad
Univ. Lille, CNRS, Centrale Lille,
Univ. Polytechnique Hauts-de-France,
UMR 8520 - IEMN
Villeneuve d'Ascq, France
ali.mourad.etu@univ-lille.fr

Ludovic Burgnies
Univ. Lille, CNRS, Centrale Lille,
Univ. Polytechnique Hauts-de-France,
UMR 8520 - IEMN
Villeneuve d'Ascq, France
also with the Université du Littoral
Côte d'Opale, F-62228 Calais, France
ludovic.burgnies@univ-lille.fr

Éric Lheurette
Univ. Lille, CNRS, Centrale Lille,
Univ. Polytechnique Hauts-de-France,
UMR 8520 - IEMN
Villeneuve d'Ascq, France
eric.lheurette@univ-lille.fr

A thin coding metasurface was produced with 8*8 random configurations formed of two elements, encoded as element "0" and element "1", with a phase difference equals to 180±30° in a broad frequency band from 28 to 40 GHz. An optimal coding metasurface allowed to reduce the monostatic and bistatic Radar Cross Section (RCS) below -10 dB from 28 to 40 GHz when compared to a perfect electric conductor (PEC) plate with same size. The coupling effect produced between the elements has been reduced. The optimal random coding metasurface was designed by using an efficient method of minimization called "pattern search" with the help of planar array theory, and simulated by means of the CST Microwave Studio software.

I. INTRODUCTION

At the beginning of the 21^{st} century, the concept of metamaterial has introduced new perspectives to manipulate the propagation of waves [1]. The metamaterial which is composed of sub-wavelength resonant particles can be considered as an effective medium characterized by constitutive parameters (permittivity and permeability), that can take values much higher or lower than unity, or even negative [2]. This property offers a promising future for several application areas such as imaging, polarization and antenna radiation control, and electromagnetic wave absorption. In recent years, great efforts both in academic and engineering field has been dedicated to own an extraordinary capability in the electromagnetic (EM) waves manipulations at the microwave [3], terahertz [4] and optical [5] frequencies. Metamaterials are of great interest in various domains such as many applications such as perfect absorber [6][7][8], invisible cloaking [3][9], surface plasmon polariton [10][11], polarization rotation surface (PRS) [12], Artificial Magnetic Conductor (AMC), or antennas [13]. A two-dimensional (2-D) metamaterial [14] called metasurface, offers several advantages over the volume metamaterials. From the physical point of view, the small thickness of the metasurface limits the penetration of the electromagnetic wave, which reduces the losses inherent to the interaction with resonant inclusions.

The generalized Snell's law which explains the anomalous phenomenon of the refractions and reflections in the presence of a phase gradient [5], inspired the physicists to achieve polarization conversion [15], lensing [16], and conversion of propagating wave to surface wave [17]. One of the important applications of metasurfaces, especially in the military fields, is to reduce the Radar Cross Section (RCS) of an object. Recently, with the strong evolution of the radar detectors, electromagnetic (EM) stealth has become a very important target. Generally, there are two different ways to do that, one of them is the absorption method which transforms the incident energy into heat [18][19][20], and the other one is reshaping the scattering pattern to redirect the incident EM energy to one or several directions out of the detector angular range. The AMC was first introduced by Sievenpiper et al. in 1999 [21]. In 2007, Paguay et al. succeeded to scatter the reflected energy into four directions and then reduce, approximately to zero, the RCS in the normal direction, by arranging perfect electric conductor PEC and artificial magnetic conductor AMC as a chessboard structure [22]. In 2013, Zhao combined two kinds of AMC, reducing by that the RCS in large band of frequencies [23]. In 2014, Cui et al. proposed for the first time the concepts of "coding metamaterial", "digital metamaterial" and "programming metamaterial" to manipulate the EM waves [24].

In designs, the 1-bit coding is a binary array composed of "0" and "1" elements synthesized of 180° phase difference. By arranging these elements in a particular way the scattering fields are manipulated in order to obtain different functionalities. Overall, the coding bits can be achieved by binary phases, or even binary polarizations. Also, in 2014, Wang et al. proposed a low-scattering metasurface by using the particle swarm optimization (PSO) algorithm with the far-field scattering pattern to predict an optimal configuration [25]. In 2015, a terahertz metasurface was proposed to produce ultralow reflections across a broad-frequency spectrum and wide incidence angles by controlling the reflection phases of subwavelength structures [26].

In this present paper, we take the advantage of new perspectives of coding metasurfaces [24] to reduce the RCS in both monostatic and bistatic directions at microwave spectra from 26 to 40 GHz.

II. THEORETYCAL FORMALISM AND EQUATIONS

A coding metasurface is an array of $M \times N$ areas of size $D_x \times D_y$ where each of them is characterized by a reflection coefficient Γ_{pq}. Areas are called elements and they are produced by a periodic sub-array of $m \times n$ unit-cells with periods a_x and a_y, very small when compared to the free-space wavelength λ_0 of the incident wave ($\lambda_0 = c/f$, where c is the speed of light in vacuum and f the frequency) (see Fig. 1).

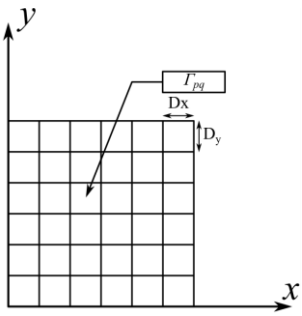

Fig. 1. Scheme of a coding metasurface composed of an array of $M \times N$ areas of size $D_x \times D_y$. The area at a (p, q) position is characterized by a reflection coefficient Γ_{pq}.

The RCS of a rectangular metasurface, under normal incidence plane wave, can be deduced from the far-field pattern function $f(\theta, \phi)$.

$$RCS^{Ms} \propto |f(\theta,\phi)|^2 \quad (1)$$

The pattern function $f(\theta, \phi)$ of the coding metasurface can be expressed by

$$f(\theta,\phi) = E_P . A_F \quad (2)$$

With E_p the element pattern and A_F the array factor. The concept of E_p and A_F is explained by the principle of planar array theory [27].

The element pattern E_p can be expressed

$$E_P = \left[\frac{1}{m}\frac{sin\left(\frac{m}{2}\psi_x\right)}{sin\left(\frac{\psi_x}{2}\right)}\right]\left[\frac{1}{n}\frac{sin\left(\frac{n}{2}\psi_y\right)}{sin\left(\frac{\psi_y}{2}\right)}\right]$$

Where

$$\psi_x = 2\pi\frac{a_x}{\lambda_0}sin(\theta)cos(\phi)$$

$$\psi_y = 2\pi\frac{a_y}{\lambda_0}sin(\theta)sin(\phi)$$

As the periods a_x and a_y of the sub-array unit-cells are very small compared to the free-space wavelength λ_0 ($a_x/\lambda_0 << 1$ and $a_y/\lambda_0 << 1$), the element pattern can be rewritten as

$$sin\left(\frac{\psi_x}{2}\right) \approx \frac{\psi_x}{2}$$

$$E_P = \left[\frac{sin(X)}{X}\right]\left[\frac{sin(Y)}{Y}\right] \quad (3)$$

Where

$$X = \pi\frac{m\,a_x}{\lambda_0}sin(\theta)cos(\phi) = \pi\frac{D_x}{\lambda_0}sin(\theta)cos(\phi)$$

$$Y = \pi\frac{n\,a_y}{\lambda_0}sin(\theta)sin(\phi) = \pi\frac{D_y}{\lambda_0}sin(\theta)sin(\phi)$$

Then, the array factor A_F can be expressed by

$$A_F = \sum_{p=1}^{M}\sum_{q=1}^{N} \Gamma_{pq}\, e^{j\{2(p-1)X+2(q-1)Y\}} \quad (4)$$

The normalization function N_{RCS} of a coding metasurface is a function allowing to evaluate its performance in comparison with the maximum RCS achieved for a perfect conductor (PEC) plate with the same size and under normal incident plane wave.

$$N_{RCS}(\theta,\phi) = \frac{RCS^{Ms}}{RCS^{PEC}_{max}} \quad (5)$$

The PEC plate can be described as a coding metasurface with $\Gamma_{pq} = \Gamma = -1 \;\; \forall\, (p, q)$. For a plane wave in normal incidence, the maximum RCS is observed in the backscattering direction ($\theta = 0$).

$$RCS^{PEC}_{max} \propto (M \times N)^2 \quad (6)$$

By introducing equations (1) and (6) in (5), the normalization function can be rewritten

$$N_{RCS}(\theta,\phi) = \frac{|f(\theta,\phi)|^2}{(M \times N)^2} \quad (7)$$

For a plane wave in normal incidence, the monostatic RCS reduction is defined as the normalization function in the backscattering direction ($\theta = 0$).

$$RCS^{mono}_{reduction} = \frac{1}{(M \times N)^2}\left|\sum_{p=1}^{M}\sum_{q=1}^{N} \Gamma_{pq}\right|^2 \quad (8)$$

$$RCS^{mono}_{reduction} = \frac{1}{(N_0 + N_1 + \cdots)^2}|\, N_0\, \Gamma_0 + N_1\, \Gamma_1 + \cdots|^2 \quad (9)$$

Where N_0, N_1, N_2 etc…, represent, respectively, the numbers of elements of value "0", "1", "2" etc…, and Γ_0, Γ_1, Γ_2 etc…, are the reflection coefficient of these elements. Equation (9) shows that the monostatic RCS reduction is independent on the size of the elements D_x and D_y, but only depends on the number of each type of elements N_i and its reflection coefficient Γ_i.

The bistatic RCS reduction is defined as the maximum of the normalization function when the overall direction (θ, ϕ) is considered.

$$RCS^{bi}_{reduction} = max[N_{RCS}(\theta,\phi)]_{\theta,\phi} \quad (10)$$

For a 1-bit coding metasurface which consists of a combination of N_0 elements "0" and N_1 elements "1" of size $D_x \times D_y$, and reflection coefficient Γ_0 and Γ_1, respectively, the monostatic RCS reduction becomes

$$RCS^{mono}_{reduction} = \frac{1}{(N_0 + N_1)^2}|\, N_0\, \Gamma_0 + N_1\, \Gamma_1|^2 \quad (11)$$

III. Design and Numerical Analysis of a 1-bit Diffuse Metasurface

A squared 1-bit coding metasurface is illustrated in Fig. 2a. This metasurface consists of a combination of equal size squared "0" and "1" elements with dimension D. Each element is designed for achieving a 180±30° phase difference between reflected wave from each other with approximately the same magnitude in order to achieve a high scattering. Whereas perfect metamaterial absorbers involve periodic or random patterns in order to absorb the Electromagnetic (EM) energy, the 1-bit coding metamaterials diffuse or redirect EM energy by means of different encoding sequences (arrangement) of "0" and "1" elements. The element combination produces EM interferences and redirects the wave in non-specular directions. For example, under a periodic configuration of 0101...01/0101...01/... shown in Fig. 2b the normal incident wave is scattered toward two symmetric directions, whereas under a periodic chessboard configuration shown in Fig. 2c, 0101..01/1010..10/0101..01/.., the normal incident wave is scattered toward four symmetric directions. As a generality, the element combination in a particular way can diffuse the incident EM energy toward different directions. By increasing the number of the reflected directions, the EM energy reflected in each direction can be decreased, making a significant RCS reduction.

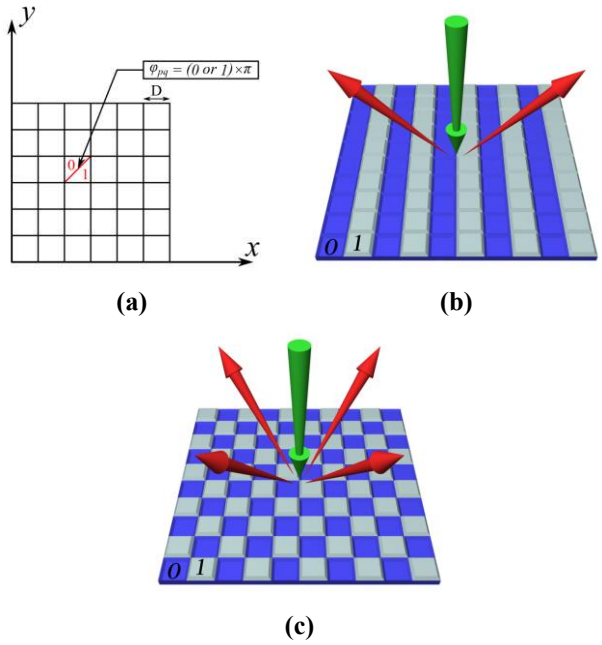

Fig. 2. **(a)** Scheme of a squared coding metasurface composed of an array of $N \times N$ squared areas of size D corresponding to a "0" or "1" element. Illustration of the reflected wave by a coding metasurface with a periodic 0101...01/0101...01/... configuration **(b)**, and with a chessboard configuration **(c)**.

A. Unit-cell and element design

The unit-cells being dimensioned with respect to long wavelength regime, the definition constraints are quite low and a wide variety of geometries can be considered. Here, we focused on the isotropic unit-cell shown in Fig. 3a which is expected to be weakly sensitive to the azimuth angle of the incident wave.

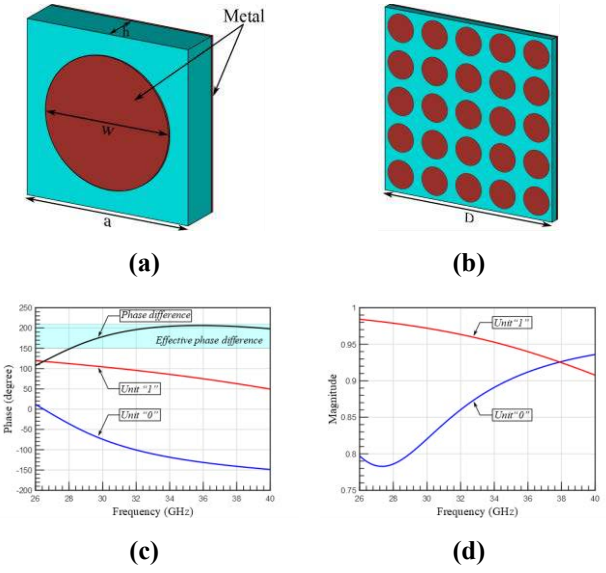

Fig. 3. Illustration of the unit-cell **(a)** and of a periodic array of 5 × 5 unit-cells producing the "0" and "1" elements **(b)**. Phases **(c)** and magnitudes **(d)** of the reflection coefficient of the unit-cells producing the "0" and "1" element.

Two unit-cells structures were designed to realize 1-bit coding metasurfaces under normal incidence targeting a broad frequency band. This design work was carried out by means of the CST Microwave Studio software by applying the finite element method (frequency solver) with periodic conditions in order to determinate the reflection coefficients. The two unit-cells are encoded as unit "0" and unit "1". A circular metallic patch printed on a back-grounded FR4 dielectric substrate, with permittivity ($\varepsilon_r = 3.75(1 - j0.05)$ at 26 GHz) was considered for both the "0" and "1" units (see Fig. 3a). The thickness of the substrate was $h = 0.755$ mm. The metallic patch has a thickness of 30 µm with a width $w = 2.3$ mm for the unit "0" and 1 mm for the unit "1". The period of the unit cell is $a = 3$ mm. A phase difference 180±30° between the units "0" and "1" is achieved in a broad frequency band from 28 GHz to 40 GHz, and the phase difference is exactly 180° at 30.2 GHz (see Fig. 3c). Also, we can note that the two units are highly reflective with a magnitude of the reflection coefficient higher than 0.78 for both the "0" and "1" units in the frequency band 28-40 GHz.

For a coding metasurface, the coupling between different adjacent elements can affect the reflection response of the elements themselves. Then the RCS reduction of the coding metasurface can be lower than expected. Here, we analyze the influence of the coupling effect on the RCS reduction of a coding metasurface by considering the chessboard configuration. This is the configuration with the highest coupling issue due to adjacent "0" and "1" elements. As illustrated in Fig. 4a, an element "0" composed of 5 × 5 unit-cells with $w = 2.3$ mm is surrounding by 4 elements "1" with $w = 1$ mm, and conversely. Therefore, the reflection coefficient of the element "0" can be affected by the 4 different neighboring elements. For a random configuration, the number of different neighboring elements will be lower than 4. In order to evaluate the coupling effect, we can compare together analytic results calculated by (11) and the simulation results of a complete coding metasurface. Actually, the analytic formula does not take into account the coupling effect which is considered in other hand by a simulation of the complete coding metasurface by means of *CST* software. Thus, a good agreement between the monostatic RCS reduction calculated by (11) and the simulated one means there is low coupling effect between elements.

A comparison of the RCS reduction calculated by (11) and simulated by *CST* is shown in Fig. 4 when the number n of unit-cells per element is varied from 1 to 5. The analytic results were obtained by introducing in equation (11) the simulated complex reflection coefficient of the "0" and "1" units as shown in Fig. 3c and Fig. 3d. The simulation of the RCS was carried out by means of CST by applying the time domain solver to the full structure bounded by open (add space) conditions under a normal incident plane wave. The simulated RCS was normalized by the maximum of RCS of a PEC plate with same size L and under normal incident plane wave, expressed by

$$RCS_{max}^{PEC} = \frac{4\pi A^2}{\lambda_0^2} \qquad (8)$$

where $A = L \times L$ is the area of the PEC plate. Comparison was produced by considering metasurfaces with a quasi-constant size $L \times L$, with $L = 90$ mm and 96 mm for $n = 1, 3, 5$ and $n = 2, 4$, respectively. The small difference of the metasurface size between an even and odd number of unit-cells allow to realize for all values n a complete chessboard sequence 010...01/101...10/... that is in order to have an even number N of elements. Finally, we can note that the size

$D = n \times a$ of each element is enlarged by increasing the number n of unit-cell per element. Thus for the metasurface shown in Fig. 4a $n = 5$, $N = 6$, $D = 15$ mm, and $L = 90$ mm.

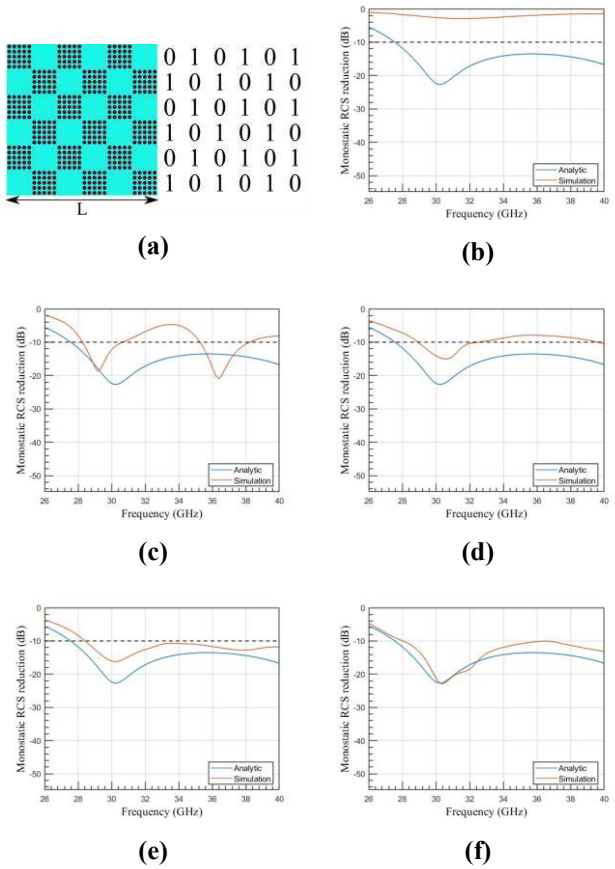

Fig. 4. **(a)** Illustration of a squared chessboard metasurface of size $L \times L$. **(b) (c) (d) (e)** and **(f)** Simulated and analytic responses of the monostatic RCS reduction under normal incidence plane wave of a chessboard configuration with $n = 1, 2, 3, 4$ and 5, respectively.

As expected (see comment about equation (9)), the analytic RCS reduction plotted in Fig. 4b,c,d,e,f is independent on the element size D and consecutively independent on the number n. For $n = 1$, the simulated RCS reduction plotted in Fig. 4b is close to 0 and clearly different from the analytic one. That means the coupling effect between elements drastically changes the resonance behavior of the unit-cells and equation (11) doesn't predict correctly the RCS reduction. We can see that the simulated RCS reduction increases with n. For $n = 4$, the analytic and simulated RCS responses have similar trend but $n = 5$ is required to fit correctly the simulated RCS reduction by equation (11). Therefore, the chessboard metasurface with $n = 5$ shows a good agreement between the analytic monostatic RCS reduction and simulation.

With low coupling effect, polarization dependence of the diffuse metasurface on the RCS reduction response is directly related to the symmetry of the elements, and it is not related to the symmetry of the diffuse metasurface. Therefore, the incident wave polarization will not affect the RCS response of a random configuration with symmetrical elements. Therefore, the RCS will be correctly fit by the analytic approximation where each element reflects as an isolated pixel. In this case, an agreement between the analytic and simulated RCS reduction will be strong. That promotes to use the analytical formula in the prediction process of the optimal configurations able to reduce the RCS in all directions.

B. 1-bit diffuse metasurface design

In the construction process of the diffuse configuration, the metasurface is first designed with respect to the parameters a, n and N, as $L = N \times n \times a$. The first two parameters, a and n, are set as 3 mm and 5 in section 3A. Then, N can be calculated.

The diffusion degree of the EM energy, and then of the RCS reduction, is somehow related to the disorder degree of the "0" and "1" elements [28], which can be significant with high number of elements $N \times N$. Therefore, there is a strong correlation between the level of the RCS reduction and the value of N [24]. Thus, $N = 8$ is chosen in order to acquire a high reduction in the RCS together with simulation and experimental constraints. The former is concerned with the computer resource (as memory limitation) and the later with practical limitation in experiments as a sufficient distance between the antenna and the sample in order to insure a planar incident phase front on the surface of the sample.

In summary, $n = 5$, $a = 3$ mm, and $N = 8$ are chosen carefully in order to acquire a high reduction in RCS respecting the simulation and experimental constraints and low coupling between elements.

Since the diffusion degree can be significant for a high number of elements $N \times N$, it is very challenging to minimize the RCS reduction formula (see equation (10)) due to the strong discretization involved and time consuming process. The time consuming process is due to the high degrees of freedom $N \times N$, which is $2^{N \times N}$ possible configurations in the case of 1-bit coding. Therefore, an efficient method of minimization called "pattern search" is applied to address the minimum of RCS rapidly. In order to find the global minimum of RCS, we first consider typically 2000 starting random configurations. Then the optimization algorithm searches an optimal random configuration for each starting configuration. Then, the best one is selected. An extended explanation of the pattern search optimization can be found in [29]. For the sake of illustration, a selected optimal coding metasurface with random configuration is shown in Fig. 5. Finally, the RCS reduction of the metasurface is simulated in order to achieve the frequency response and the RCS pattern.

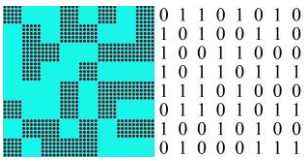

Fig. 5. An 8 × 8 optimal configuration predicted by the "pattern search" optimization algorithm.

C. Numerical analysis

The monostatic RCS reduction for a chessboard and the optimal configuration shown in Fig. 5 was simulated and is shown in Fig. 6a and 6b, respectively. The highest reduction is observed at 30.2 GHz with a RCS reduction around -20 and -50 dB for the chessboard and optimal configurations, respectively. That corresponds to a phase difference exactly equals to 180° producing the highest destructive interferences. On the other hand, the bistatic RCS reduction plotted in Fig.

6a and 6b shows a higher performance of the optimal random configuration compared with the chessboard one with a -15 dB reduction when the phase difference is in the range of 180±13°.

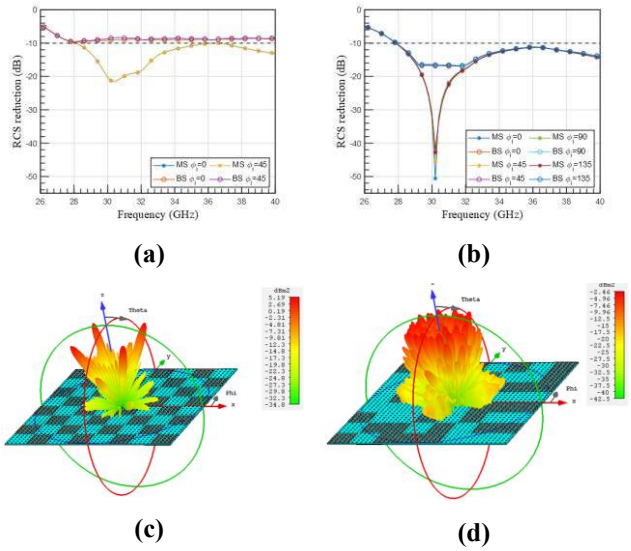

Fig. 6. Simulated RCS reduction response in the monostatic (MS) and bistatic (BS) direction for different azimuth angles (ϕ_i) for a 8×8 chessboard metasurface **(a)** and for an optimal random configuration **(b)**. RCS pattern for the 8×8 chessboard metasurface **(c)** and the optimal random configuration **(d)** simulated at 30.2 GHz under normal incidence and for an x-polarized wave ($\phi_i = 0$).

To sum up, the optimal random configuration shows a good improvement in the RCS reduction compared with the chessboard in both monostatic and bistatic directions with a ratio lower than -10 dB over a broad frequency band from 28 to 40 GHz. In Fig. 6a and Fig. 6b, it can be seen that the performance of the optimal random configuration is insensitive to the azimuth angle of the incident wave under normal incidence.

IV. Fabrication and Experiments

For the experimental section, digital metasurfaces were fabricated with Printed Circuit Board (PCB) technologies widely tested in the field of microwaves. For the manufacturing stage, common photolithography and chemical etching were used. The substrate was FR4.

The experimental characterization of the structures were carried out in free space by means of a horn antenna and a Vector Network Analyzer (VNA) which preserves phase information. This phase information appears to be essential for time gating filtering in order to suppress unwanted reflection in the measured reflection before calculating the RCS reduction. The sample and the horn antenna were separated by around 145 cm in order to illuminate the sample by a plane wave (far-field condition). This distance was calculated for a size of the sample 12×12 cm^2. A metallic plate (12×12 cm^2) was used as reference.

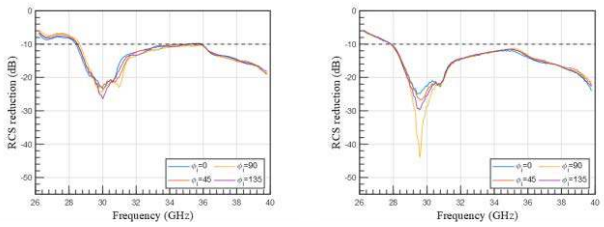

Fig. 7. Monostatic RCS reduction measured under normal incidence plane wave for the chessboard **(a)** and the optimal random configuration **(b)**.

Experimental results are in good agreement with the simulated ones in the monostatic direction for both chessboard and optimal configurations (see Fig 7a and Fig 7b). Especially, a monostatic RCS reduction lower than -10 dB is measured in the frequency band 28-40 GHz and it is insensitive to the azimuth angle of the normal incident wave. The small mismatch between the experimental and simulated results can be mainly attributed to an imperfect plane wave impinging on the surface of samples in experiments (sample not far enough).

V. Conclusion

In summary, a thin diffuse metasurface is proposed, simulated, fabricated, and tested. Using the planar array theory and "pattern search" algorithm, an optimal diffuse array is obtained. A RCS reduction higher than -10 dB compared to a metallic plate with same size in both monostatic and bistatic directions is achieved. The diffuse metasurface has been designed by means of basic unit cell and low coupling effect, and it operates over a broad frequency band from 28 to 40 GHz.

Acknowledgment

Ali Mourad would like to thank the "Direction Générale de l'Armement" (DGA) for the funding of his PhD thesis. The authors would like to thank the characterization platform CHOP of IEMN. This work was financially supported by the French Agence Nationale de la Recherche by means of the ANR MESANGES project, ANR-20-CE25-0016.

References

[1] E. Lheurette, *Metamaterials and Wave Control*. John Wiley & Sons, 2013.
[2] D. R. Smith, W. J. Padilla, D. C. Vier, S. C. Nemat-Nasser, and S. Schultz, "Composite Medium with Simultaneously Negative Permeability and Permittivity," *Phys. Rev. Lett.*, vol. 84, no. 18, pp. 4184–4187, May 2000, doi: 10.1103/PhysRevLett.84.4184.
[3] D. Schurig *et al.*, "Metamaterial Electromagnetic Cloak at Microwave Frequencies," *Science*, vol. 314, no. 5801, pp. 977–980, Nov. 2006, doi: 10.1126/science.1133628.
[4] L. Liang *et al.*, "Anomalous Terahertz Reflection and Scattering by Flexible and Conformal Coding Metamaterials," *Adv. Opt. Mater.*, vol. 3, no. 10, pp. 1374–1380, Oct. 2015, doi: 10.1002/adom.201500206.
[5] N. Yu *et al.*, "Light Propagation with Phase Discontinuities: Generalized Laws of Reflection and Refraction," *Science*, vol. 334, no. 6054, pp. 333–337, Oct. 2011, doi: 10.1126/science.1210713.
[6] N. I. Landy, S. Sajuyigbe, J. J. Mock, D. R. Smith, and W. J. Padilla, "A Perfect Metamaterial Absorber," *Phys. Rev. Lett.*, vol. 100, no. 20, p. 207402, May 2008, doi: 10.1103/PhysRevLett.100.207402.
[7] X. Shen *et al.*, "Triple-band terahertz metamaterial absorber: Design, experiment, and physical interpretation," *Appl. Phys. Lett.*, vol. 101, no. 15, p. 154102, Oct. 2012, doi: 10.1063/1.4757879.
[8] N. Fernez *et al.*, "Radiative Quality Factor in Thin Resonant Metamaterial Absorbers," *IEEE Trans. Microw. Theory Tech.*, vol. 66, no. 4, pp. 1764–1772, Apr. 2018, doi: 10.1109/TMTT.2017.2784808.

[9] T. Ergin, N. Stenger, P. Brenner, J. B. Pendry, and M. Wegener, "Three-Dimensional Invisibility Cloak at Optical Wavelengths," *Science*, vol. 328, no. 5976, pp. 337–339, Apr. 2010, doi: 10.1126/science.1186351.
[10] J. B. Pendry, "Mimicking Surface Plasmons with Structured Surfaces," *Science*, vol. 305, no. 5685, pp. 847–848, Aug. 2004, doi: 10.1126/science.1098999.
[11] A. Ghaddar, É. Lheurette, and L. Burgnies, "Wireless Experimental Determination of Dispersion Curves of Spoof Surface Plasmon Polariton Modes Supported by a Transmission Line," *Phys. Status Solidi B*, vol. 258, no. 6, p. 2100003, 2021, doi: 10.1002/pssb.202100003.
[12] K. Kärkkäinen and M. Stuchly, "Frequency selective surface as a polarisation transformer," *IEE Proc. - Microw. Antennas Propag.*, vol. 149, no. 5, pp. 248–252, Dec. 2002, doi: 10.1049/ip-map:20020576.
[13] J. Hao, A. Djouadi, F. Rault, X. Tao, É. Lheurette, and L. Burgnies, "Multiresonant Split Ring Resonator with Meandered Strips," *Phys. Status Solidi A*, vol. 217, no. 6, p. 1901017, 2020, doi: 10.1002/pssa.201901017.
[14] C. L. Holloway, E. F. Kuester, J. A. Gordon, J. O'Hara, J. Booth, and D. R. Smith, "An Overview of the Theory and Applications of Metasurfaces: The Two-Dimensional Equivalents of Metamaterials," *IEEE Antennas Propag. Mag.*, vol. 54, no. 2, pp. 10–35, Apr. 2012, doi: 10.1109/MAP.2012.6230714.
[15] X. Ma, C. Huang, M. Pu, C. Hu, Q. Feng, and X. Luo, "Multi-band circular polarizer using planar spiral metamaterial structure," p. 9, 2012.
[16] X. Chen *et al.*, "Dual-polarity plasmonic metalens for visible light," *Nat. Commun.*, vol. 3, no. 1, p. 1198, Jan. 2012, doi: 10.1038/ncomms2207.
[17] S. Sun, Q. He, S. Xiao, Q. Xu, X. Li, and L. Zhou, "Gradient-index meta-surfaces as a bridge linking propagating waves and surface waves," *Nat. Mater.*, vol. 11, no. 5, pp. 426–431, May 2012, doi: 10.1038/nmat3292.
[18] O. Luukkonen, F. Costa, A. Monorchio, and S. A. Tretyakov, "A Thin Electromagnetic Absorber for Wide Incidence Angles and Both Polarizations," *IEEE Trans. Antennas Propag.*, vol. 57, no. 10, pp. 3119–3125, Oct. 2009, doi: 10.1109/TAP.2009.2028601.
[19] F. Costa, A. Monorchio, and G. Manara, "Analysis and Design of Ultra Thin Electromagnetic Absorbers Comprising Resistively Loaded High Impedance Surfaces," *IEEE Trans. Antennas Propag.*, vol. 58, no. 5, pp. 1551–1558, May 2010, doi: 10.1109/TAP.2010.2044329.
[20] C. M. Watts, X. Liu, and W. J. Padilla, "Metamaterial Electromagnetic Wave Absorbers," *Adv. Mater.*, vol. 24, no. 23, pp. OP98–OP120, Jun. 2012, doi: 10.1002/adma.201200674.
[21] D. Sievenpiper, Lijun Zhang, R. F. J. Broas, N. G. Alexopolous, and E. Yablonovitch, "High-impedance electromagnetic surfaces with a forbidden frequency band," *IEEE Trans. Microw. Theory Tech.*, vol. 47, no. 11, pp. 2059–2074, Nov. 1999, doi: 10.1109/22.798001.
[22] M. Paquay, J.-C. Iriarte, Iñ. Ederra, R. Gonzalo, and P. de Maagt, "Thin AMC Structure for Radar Cross-Section Reduction," *IEEE Trans. Antennas Propag.*, vol. 55, no. 12, pp. 3630–3638, Dec. 2007, doi: 10.1109/TAP.2007.910306.
[23] Y. Zhao, X. Cao, J. Gao, and W. Li, "Broadband radar absorbing material based on orthogonal arrangement of CSRR etched artificial magnetic conductor," *Microw. Opt. Technol. Lett.*, vol. 56, no. 1, pp. 158–161, 2014, doi: 10.1002/mop.28033.
[24] T. J. Cui, M. Q. Qi, X. Wan, J. Zhao, and Q. Cheng, "Coding metamaterials, digital metamaterials and programmable metamaterials," *Light Sci. Appl.*, vol. 3, no. 10, pp. e218–e218, Oct. 2014, doi: 10.1038/lsa.2014.99.
[25] K. Wang, J. Zhao, Q. Cheng, D. S. Dong, and T. J. Cui, "Broadband and Broad-Angle Low-Scattering Metasurface Based on Hybrid Optimization Algorithm," *Sci. Rep.*, vol. 4, no. 1, p. 5935, May 2015, doi: 10.1038/srep05935.
[26] D. S. Dong *et al.*, "Terahertz Broadband Low-Reflection Metasurface by Controlling Phase Distributions," *Adv. Opt. Mater.*, vol. 3, no. 10, pp. 1405–1410, Oct. 2015, doi: 10.1002/adom.201500156.
[27] C. A. Balanis, *Antenna Theory: Analysis and Design*. John Wiley & Sons, 2015.
[28] T.-J. Cui, S. Liu, and L.-L. Li, "Information entropy of coding metasurface," *Light Sci. Appl.*, vol. 5, no. 11, pp. e16172–e16172, Nov. 2016, doi: 10.1038/lsa.2016.172.
[29] A. Mourad, L. Burgnies, and E. Lheurette, "Broadband RCS reduction by mean of disordered coded metasurfaces," *Submitted for publication*.